climate

MDPI

Article

Multicriteria Spatial Modeling: Methodological Contribution to the Analysis of Atmospheric and Surface Heat Islands in Presidente Prudente, Brazil

Danielle Cardozo Frasca Teixeira [1,*] and Margarete Cristiane de Costa Trindade Amorim [2]

[1] National Council for Scientific and Technological Development (CNPq), São Paulo State University (Unesp), School of Technology and Sciences, Presidente Prudente 19060-900, Brazil
[2] Department of Geography, São Paulo State University (Unesp), School of Technology and Sciences, Presidente Prudente 19060-900, Brazil; margarete.amorim@unesp.br
* Correspondence: danielle.frasca@unesp.br; Tel.: +55-18-98128-5368

Abstract: Several studies demonstrate the potential of models for the representation of phenomena such as urban heat islands. This article aimed to analyze atmospheric heat islands (UHI_{ucl}) by integrating primary air temperature data with spatial information such as land use and relief from a multicriteria model based on multiple linear regression. Furthermore, we compared the measured and estimated air temperature at 11 p.m. with the surface temperature at 10:51 p.m. (local time). These temperatures were obtained through the thermal band of the Landsat 8 satellite considering extraction points of interest in Presidente Prudente city, Brazil. The multicriteria model showed reliability in UHI_{ucl} spatialization, reaching the confidence interval (p-value ≤ 0.05). The model proves that urban surface materials are the main energy sources modulating heat transfer to the atmosphere, while vegetation has a temperature-reducing effect. Precise mappings such as the one proposed here are relevant for the formulation of measures that support decision-making by public authorities. These mappings aim at urban planning that is resilient to the effects of urban climate and can be replicated in other realities.

Keywords: urban climate; urban canopy heat island; surface heat island; land use; vegetation; multicriteria modeling

Citation: Teixeira, D.C.F.; Amorim, M.C.d.C.T. Multicriteria Spatial Modeling: Methodological Contribution to the Analysis of Atmospheric and Surface Heat Islands in Presidente Prudente, Brazil. *Climate* **2022**, *10*, 56. https://doi.org/10.3390/cli10040056

Academic Editor: Forrest M. Hoffman

Received: 26 January 2022
Accepted: 1 April 2022
Published: 4 April 2022

1. Introduction

The diagnosis and spatial representation of urban heat islands (UHIs) challenge the scientific community dedicated to this topic. This is mostly because the UHI phenomenon varies in time and space, and thus generalizations of its spatial representation limit real knowledge of climate characteristics at the local scale [1]. This becomes even more relevant when climate recording sites are discontinuous, which compromises spatialization reliability.

In line with concerns of this nature, contemporary studies are strongly supported by Geographic Information Systems (GIS). These systems are provided with statistical and geostatistical tools, being advantageous for integrated data treatment aiming at a detailed spatial analysis [2]. Application of these resources is increasingly present in different areas of knowledge, notably in the field of urban climatology [3,4].

For a long period, researchers associated the representation of UHI with ordinary kriging, which contributed to a spatialization that was reliable near climate recording sites but doubtful in discontinuous data areas [5,6].

Another limitation of this form of representation is that a kriging-generated statistical surface is homogeneous and does not incorporate surface heterogeneities inherent to the geography of the areas of interest, which involve construction features, vegetation, and relief. It is not interesting that these heterogeneities are omitted, as they may reveal important explanatory singularities of UHI_{ucl} formation.

In this article we opted to represent one of the most documented climatic phenomena by using the local scale [7]. The aim was to analyze atmospheric heat islands (UHI_{ucl}) by integrating primary air temperature data with spatial information (e.g., land use and relief) from a multicriteria model based on multiple linear regression to represent the variability of air temperature. We also sought to compare measured air temperature (MAT), model-estimated temperature (MET), and surface temperature (ST) by considering extraction points of interest (fixed points), benefiting from the advantageous use of night-time satellite image and simultaneous in situ data recording.

Several studies have demonstrated the potential of models to represent phenomena such as UHI_{ucl} and UHI_{surf}. Amorim et al. [8] incorporated the analysis of Rennes, France, and Presidente Prudente, Brazil, by establishing a relative comparison between the UHI_{ucl} and UHI_{surf} patterns of these cities in temperate and tropical environments.

Agathangelidis et al. (2020) [9] analyzed the statistical association between temperature and surface parameters such as impermeable surface fractions, construction fraction, and building height. These authors proved the consistent influence of the impermeable surface fraction on the Earth's surface temperature.

When analyzing urban ecological scenarios aimed at improving thermal comfort in southern Italy, Gatto et al. (2021) [10] attested to the importance of urban greenery in this context in a region with Mediterranean climate. Similar to other authors, they proved that the close relationship between built environments and thermal anomalies negatively affects human thermal comfort.

Considering this presentation framework, representing the UHI_{ucl} is a pressing need. This is because among the framework of reasons that negatively interfere with the quality of life of urban populations in tropical environments are those resulting from climate change at the local scale, especially thermal comfort variables. Urban, atmospheric (UHI_{ucl}), and surface (UHI_{surf}) heat islands [7] are the immediate effects of urban climate that compromise human health, comfort, and performance [11,12].

One can explain the genesis of urban heat island at the urban canopy level—UHI_{ucl} [13]—by the relationship between solar radiation and the Earth's surface. This relationship transits through emission, reflection, transmission, and absorption schemes, that is, the radiation balance. The differences between densely built urban features and open rural areas give birth to UHI_{ucl}, recorded under stable atmospheric conditions [13].

Urbanization interferes with this energy exchange scheme and it is thus necessary to consider the surface and heat transport to the adjacent atmosphere when investigating this phenomenon. Therefore, UHI_{ucl} is a phenomenon that varies in time and space, depending on controls such as operating atmospheric conditions, city size, differences in intraurban features, and daily and seasonal radiation cycles [13,14].

By definition, UHI_{surf} consists of temperature differences between the interface of the atmosphere and solid materials in the city, which is equivalent to the rural air–land interface [7]. This level of analysis requires the use of remote sensing from the conversion of gray levels of thermal images into pixel radiant temperature [15,16].

Several studies confirm the occurrence of the two types of UHI in Brazilian tropical cities of different population sizes [6,8,17–21]. These events have patterns of spatial distribution and peak moments different from those occurring in temperate climate cities [3,8,22].

Some Considerations about the UHI Discussion in Brazil and in the World

Discussions about urban climate phenomena have increased in Brazil since Monteiro's systemic theoretical–methodological proposal [11]. This proposal relied on the general theory of systems [23], providing climatologists with tools to study the urban atmosphere focusing on aspects such as thermal comfort, air quality, and rainfall. Since then, climate studies in Brazilian cities have been carried out focusing on the thermodynamic system and on the human perception of thermal comfort. This has to do with the typical characteristics of the tropical environment, in which heat continuously affects people [11].

Depending on the active atmospheric systems, such as the entrance of cold fronts and the Atlantic polar mass that suddenly decrease winter temperatures, the heat island can benefit populations in the sense of alleviating the effects of cold. This correlates specifically with the natural conditions of the urban terrain, in connection with thermal inversions at the valley floor [24].

Spatialization of this phenomenon is a first approach for diagnosing problems that can compromise urban thermal comfort.

These products reiterate the importance of considering climatic parameters to assess habitability and quality of life in urban areas. These parameters can improve a set of measures applicable to urban planning and at the architectural level to mitigate thermal comfort problems. Even with this recognition, what occurs in tropical cities is the restricted incorporation of this information, mainly due to lack of data or difficulty of communication between scientists and planners [25].

A common occurrence is the strong appeal to climate control in indoor environments, which adds heat to the atmosphere and increases the demand for electricity. In addition, these resources are not accessible to people with lower income, especially in underdeveloped countries [26,27].

These are the confrontations highlighted by contemporaneity that require urgent management. This situation is even more worrisome when considering notable climate changes on a local scale and the increase in the frequency of extreme weather events such as droughts, cold waves, and heat waves, which enhance the harmful effects of UHI [28].

2. Materials and Methods

The study was applied to Presidente Prudente city, western São Paulo State, Brazil. The region has Aw-type climate [29], with a dry and mild season and a hot and rainy season (Figure 1).

Presidente Prudente is a medium-sized city, whose population in the year 2021 was estimated at 231,953 by the Brazilian Institute of Geography and Statistics [30]. Economic activities in the city involve the agropastoral sector, commerce, provision of services, and educational services. Industrial activities are restricted to food and beverage, plastics, and wood and metal processing industries.

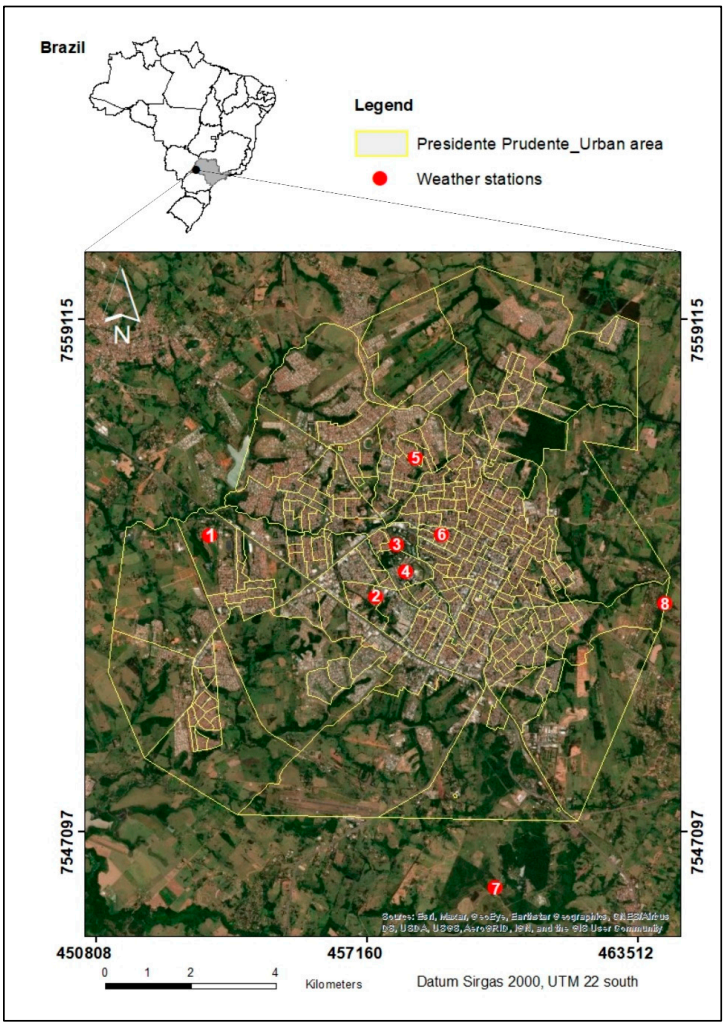

Figure 1. Location of Presidente Prudente, Brazil; measured air temperature points. Source: World Imagery, Esri (2022) [31]. Access: January 2022; IBGE Census Bureau (2010) [32].

2.1. Acquisition of Primary Data

This article investigated UHIs at the lower atmospheric/urban canopy level and at the surface level by considering the temperature of the targets [7].

In order to relate air temperature (measured and estimated) to surface temperature, we sought to extract surface temperatures by fixed points measured from the conversion of gray levels into radiant temperature [33–35]. For that, we used the thermal image of band 10 captured at night on 10 May 2020 by the Landsat 8 satellite (Table 1).

Table 1. Landsat 8 satellite images used in the study applied to Presidente Prudente (SP).

TIRS Image Presidente Prudente	Daytime	Night-Time
Applied bands	3, 4, 5	10
Point set and orbit	222/075	104/169
Date	5 April 2020	5 October 2020
Shooting time (local time)	10 h 22 a.m.	10 h 51 p.m.

Source: United States Geological Survey [36] (2021).

Modeling required the application of visible bands 3, 4, and 5 of a daytime image from the same sensor, obtained at a date close to that of the night-time thermal image, for knowledge of land use classes. In this case, we used the image obtained on 4 May 2020.

The thermal channel image was treated in the Idrisi Selva application (Clark Labs) through parameters and fixed variables extracted from the USGS website and applied through formulas. The radiometric scaling coefficients provided by the metadata file (MTL.txt) convert gray levels into radiance, and later Kelvin temperature into Celsius.

The atmospheric level of the urban canopy was obtained by monitoring air temperature from ground level to the average height of roofs and treetops [7]. For this purpose, primary air temperature data were recorded at fixed points established in representative areas of urban features and control points in the surrounding rural area [13]. Field research used Hobo data logger sensors (U23-002) protected by Hobo RS3 solar radiation shields distributed at points of interest. The equipment is typically uncertain to ±0.21 °C (0 to 50 °C) [37].

Furthermore, a Davis Instruments Vantage Pro 2 meteorological station, as well as the official station of the National Institute of Meteorology [38] and the automatic station of Universidade do Oeste Paulista (UNOESTE), provided air temperature data, totaling eight sampling points. Figure 2 shows the characteristics of these sampling points.

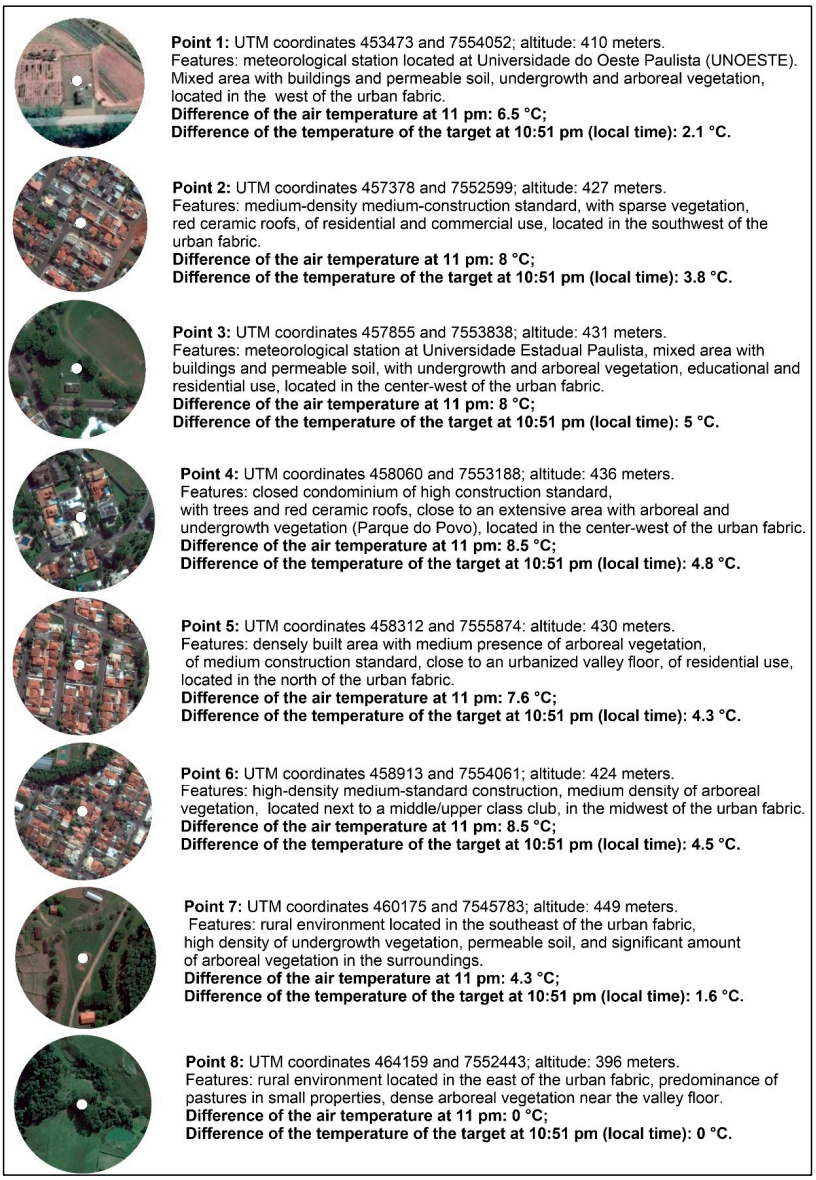

Figure 2. Characteristics of the surroundings of fixed data recording points organized in a west–east direction in Presidente Prudente. Source: Adapted from Amorim (2020) [39]; point 1: Google Earth Maps, 2021. Access: December 2021 [40].

Air temperature was recorded on May 10 at 11 p.m. (local time) to coincide with the time of the capture of the satellite image in Presidente Prudente. Data were tabulated in an Excel spreadsheet (branded by Microsoft Corporation). For presentation of the results, UHI_{ucl} and UHI_{surf} magnitudes ($\triangle T$) were obtained, using as a reference the difference between the urban and rural areas from control point 8 (from its air temperature recorded at 11 p.m. and surface temperature recorded at 10:51 p.m.), positioned in the eastern portion of the urban fabric. The definition of point 8 as a reference for the calculation of the magnitude of the UHI_{ucl} and UHI_{surf} is related to the preservation of prior-to-urbanization features, with less anthropogenic influence (forest fragment).

2.2. Multicriteria Modeling: Selection of Independent Variables

A linear multicriteria model allows per-pixel generalization of a satellite image relating land use classes, relief, and air temperature with greater reliability due to the statistical correlation between variables. Air temperature is assumed to be a dependent variable (y), while land use classes and relief are assumed to be independent variables (x), climate controls for air temperature variation [7].

Knowledge of surface heterogeneities requires mapping model input information. Land use and land cover features were revealed using multispectral visible bands of the daytime image obtained on 4 May 2020. The near-infrared band 5 and the red band 4 composed the Normalized Difference Vegetation Index (The processing of images of bands 4 and 5 provided the NDVI of the areas of interest, incorporated in the cluster classifica-tion of generation of land use and occupation classes.) (NDVI). This index was calculated by the division made after the subtraction of the near-infrared band in relation to the red band and the sum of both bands, resulting in an index ranging from -1 to 1, extremes that refer to greater (1) or less (-1) exuberance of vegetation [41].

In order to compose the chart of surface features, band 3, bands 4 and 5, and NDVI generated, by automatic unsupervised classification, a cluster chart that grouped elements of the same type and by proximity into class intervals.

The cluster functionality performed in the Idrisi application uses the one-dimensional histogram peak technique to group similar classes. Each peak groups a frequency that is considered higher than that of its side neighbors. Once the peaks are identified, the other values are assigned to the closest peak and the divisions between classes are assigned to the mean values between peaks.

Thus, an initial broad classification was performed based on seven land use classes in the study area. Taking as a reference the NDVI indices in each of these to consider the presence or absence of vegetation, a final refinement was carried out, resulting in three classes of land use and occupation in view of the prior knowledge of the study area.

The reclassification of this chart individualized land use classes for the areas of interest, identifying construction classes, exposed soils, high-vegetation areas (forest fragments, valley floors), and low-vegetation areas. This reclassification characterized the pastures present in rural surroundings, as in the study by Amorim (2020) [17].

Once the features of land use and occupation were known, per-pixel generalization was made by calculating their frequencies around air temperature measurement points. These frequencies were extracted from atmospheric observation windows expandable in proportion to the spatial resolution (30 m) of the Landsat 8 satellite. This phase allowed the generalization of spatial information and the constitution of numerical variables of the model, calculated as a function of land use features, as can be analyzed in Figure 3.

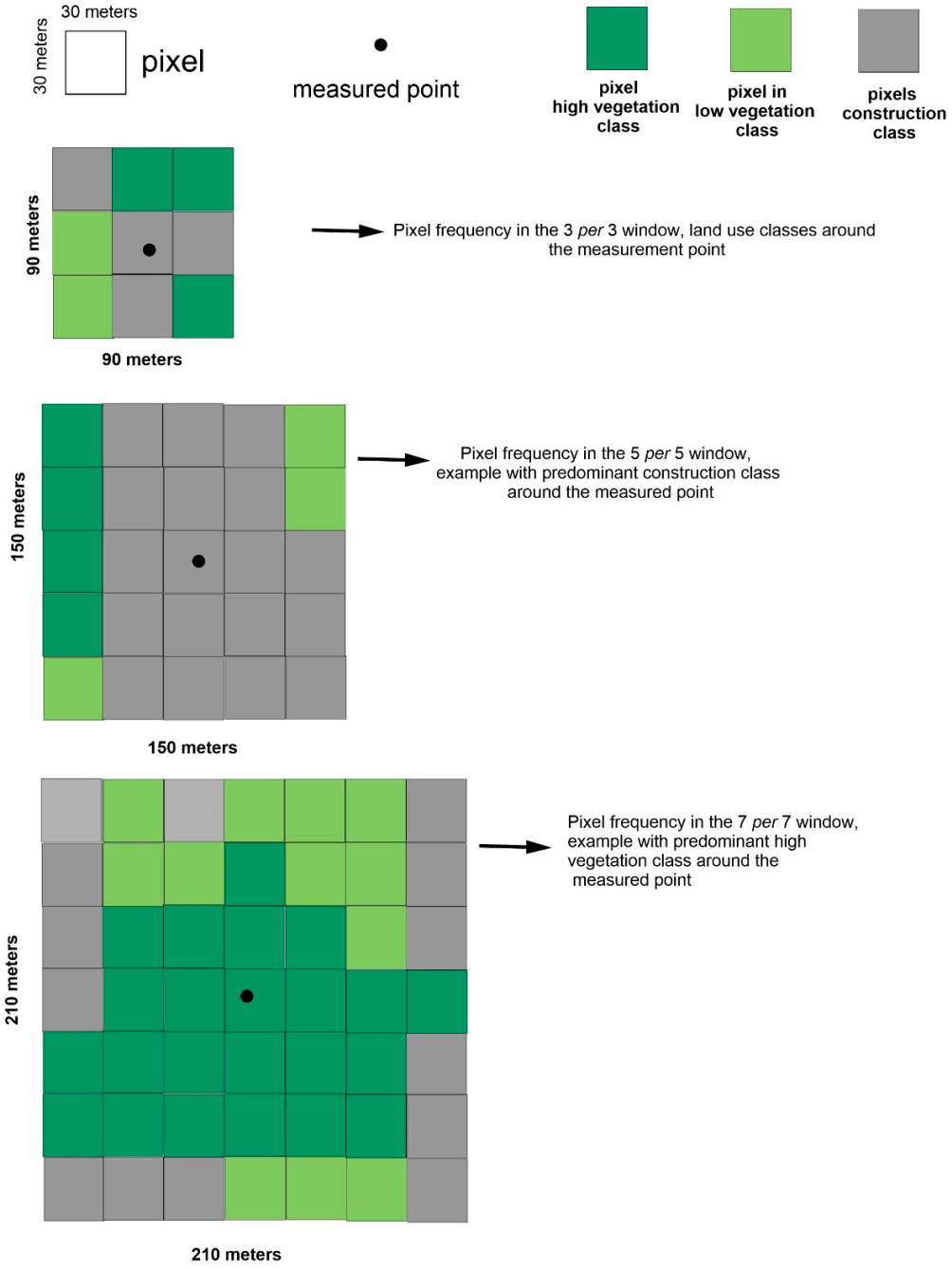

Point	Pixel total frequency around the measured fixed points 33 *per* 33 window	
	Construction class	High vegetation class
1	0	17
2	0	10
3	12	0
4	7	2
5	12	1
6	10	3
7	5	7
8	1	4

Figure 3. Calculation of pixel total frequency around the measured fixed points and generalization of spatial information. Elaborated by the authors (2022).

For the insertion of altimetric information of the terrain in the multicriteria model, a hypsometric chart was generated from images of the Shuttle Radar Topography Mission (SRTM) georeferenced in the same spatial resolution as the Landsat 8 satellite image. The extraction of the altitudes of each measured point provided the model with information on geomorphometric parameters.

Independent variables (x) resulted from cluster classification and hypsometry. These variables were incorporated into the model through their value attributes.

Recorded air temperature data were then crossed, which required the application of simple linear regression statistics. These explained the relationship between variables x (land use classes, relief) and y (air temperature), considering the fit in a scatter diagram according to the minimum square deviation method. Numerical correlation coefficients indicated whether there was a relationship between variables x and y, as well as the strength of association [42].

Each x variable has a partial coefficient, that is, a value of change in relation to the variable y obtained by simple regression. Ferreira (2014) [42] states that the analysis of values of change considers the geometric instrument and the quantitative parameter on the degree of dependence between variables that are, respectively, the regression line and the regression coefficient "***r***". The other parameter for checking dependence between variables is given by the coefficient of determination $\boldsymbol{r^2}$.

From the partial coefficients of correlation ***r*** and determination $\boldsymbol{r^2}$, we could numerically select the most important independent variables for the prediction of "y" (air temperature) while admitting urban land use classes, high vegetation, and relief. This information was crossed using the multiple linear regression function of the Idrisi application, whose global coefficient result (adjusted R^2) represented the percentage of variation that is explained by the model with the adopted variables.

The regression function resulted in the treatment formula, a mathematical representation of the relationship between variables x and y. The formula incorporated the input maps of the x variables chosen for the prediction of y, as shown in Formula (1):

$$\begin{gathered} \textit{Air temperature model} = 11.2003 + 0335 * \textit{construction class } 33 \times 33 - 0.4292 * \\ \textit{High vegetation class } 33 \times 33 + 0.0245 \textit{ Hypsometry,} \end{gathered} \quad (1)$$

where

Air temperature model is the estimated temperature;

Construction class 33 × 33 is the extrapolation per measured point of the percentage of variation of class 1 (urban) in the 33 by 33 pixel range window (990 m × 990 m);

High vegetation class 33 × 33 is the extrapolation per measured point of the percentage of variation of class 3 (high vegetation) in the 33 by 33 pixel range window;

Hypsometry refers to the altimetry value of each measured point.

The results were validated by analysis of variance (ANOVA) significance tests, through which the p-value could prove the validity of models and the global correlation between variables. For this, the significance level $\alpha \leq 0.05$ was adopted, which established a confidence interval of 95%, assuming the 5% probability of the association not to be real or random [43]. Another test performed was the F test, in which the F value was considered a parameter to determine the significance of the terms together in the model, from the same confidence interval (95%). Statistical processing was performed using the data analysis tool of the Microsoft Excel application (branded by Microsoft Corporation). Scheme 1 summarizes the sequence of procedures that involve the digital processing of images with the crossing of data recorded on the surface.

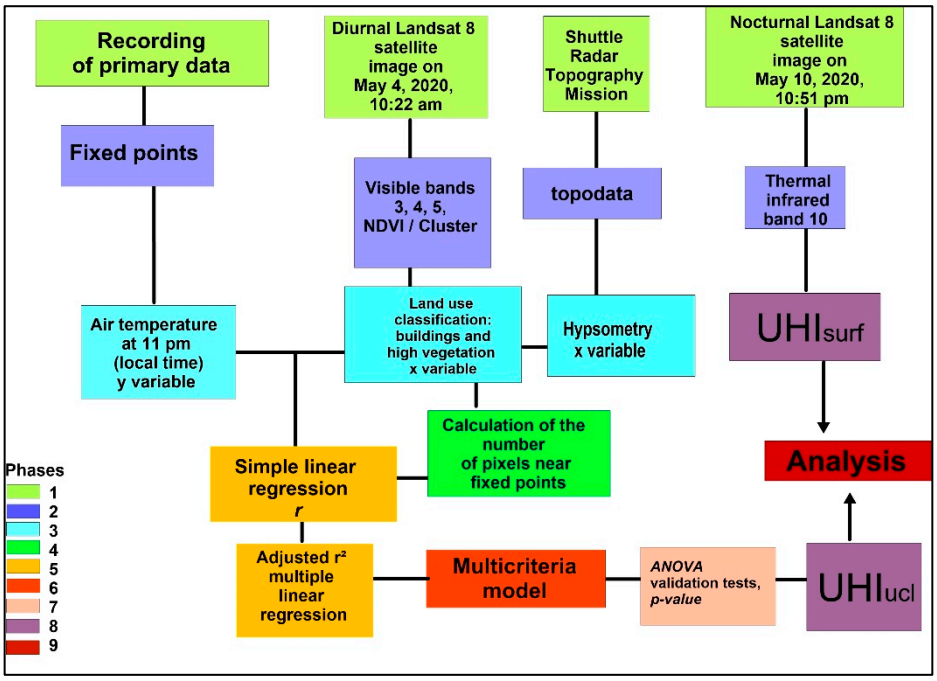

Scheme 1. Data processing phases. Elaborated by the authors (2022).

This chain of procedures resulted in a spatial model of the UHI_{ucl}, whose analysis compared the air temperature and the surface temperature extracted at fixed points, meeting the objective of the article.

3. Results

At 11:00 p.m. on 10 May 2020, the maximum and minimum spatialized atmospheric temperature were 23.5 °C and 11 °C, respectively (Figure 4). The UHI_{ucl} referenced the eastern rural area (point 8), with the highest △T of the UHI_{ucl} reaching 9 °C, clearly in construction areas. Cool islands were formed [7] that reached a △T of −1 °C on valley floors and along high-vegetation areas. Undergrowth vegetation sites showed intermediate temperatures and magnitudes. With regard to surface temperatures, the maximum temperature of the sample was 20.8 °C, occurring in central and densely built areas. The temperature of the targets decreased in peripheral urban areas. The minimum surface temperature was 10.4 °C, in areas with undergrowth and arboreal (high) vegetation, both in the bordering rural area and on valley floors, where the cores of the cool island were also formed. With △T being calculated from the extraction of the temperature of point 8, the maximum △T reached 7 °C, and the △T of the cool island reached −3 °C.

The multicriteria model with the adopted independent variables (e.g., buildings, high vegetation, and relief) explained reality with 95% reliability. Table 2 demonstrates this situation together with the results of the model validation. Despite its moderately positive correlation with air temperature, the urban class exceeded the confidence interval adopted in the composition of the model. This shows that in addition to constructive features, temperature variation depends on other climate controls of the local scale, including wind strength (At the time of recording air temperature data, the wind was at a speed of 2.5 m/s and had a southwesterly direction, inter-fering with atmospheric stability.) and unknown or unmonitored variables.

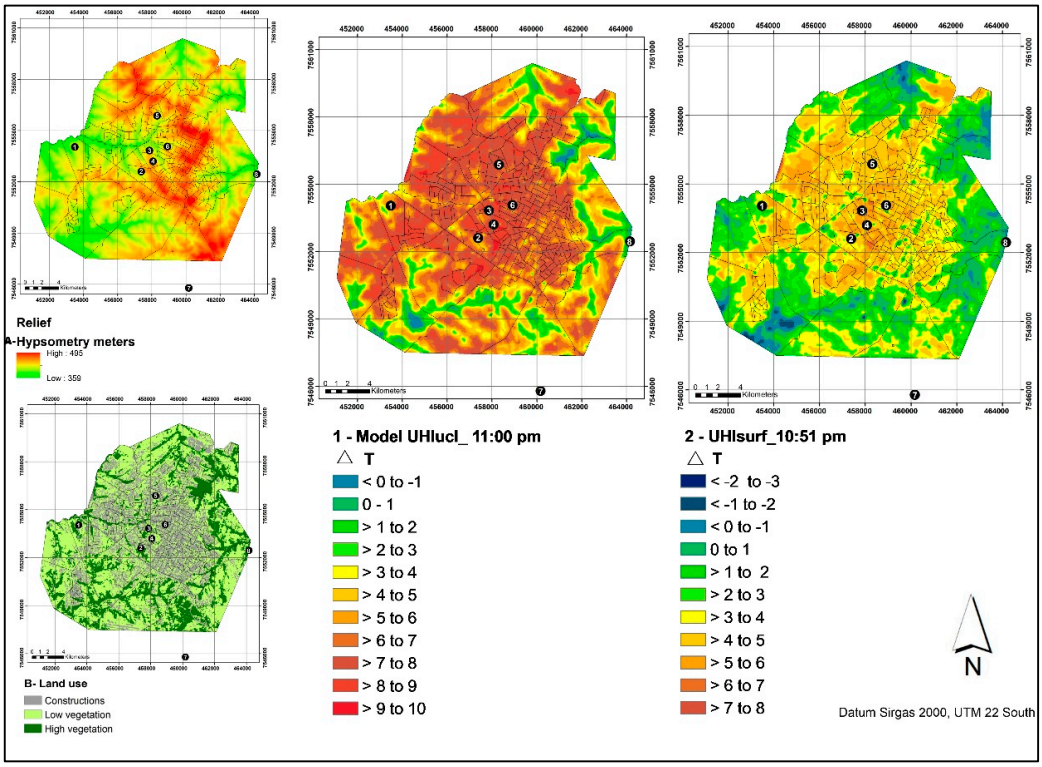

Figure 4. △T of the modelgenerated UHI_{ucl} (map 1) considering relief (detail A) and land use (detail B). △T UHI_{surf} map (map 2). Both referring to 10 May 2020, at 11:00 p.m. and 10:51 p.m. (local time), respectively, in Presidente Prudente city, Brazil. Source: USGS (2021); IBGE Census Bureau (2010). Elaborated by the authors (2022).

Table 2. Results of data validation of the spatial model considering simple and multiple linear regression and significance tests with *p*-value ($\alpha \leq 0.05$), as performed by ANOVA in Presidente Prudente, Brazil.

Presidente Prudente 33 × 33 window (990 × 990 m)			**05 October 2020 Air Temperature at 11 p.m.**	
Multicriteria model 3 variables	**r**	***p*-value**	**Significant F value**	**Adjusted R^2**
Construction class	0.73	0.62		
High vegetation	−0.93	0.03	0.000	0.80
Relief	0.56	0.00		

Data source: USGS (2021); Data recording on 10 May 2020. Organized by the authors. December 2021.

The correlation between high vegetation and air temperature is highly negative (**r** = −0.93), which clearly highlights the role of vegetation in reducing air temperature. The significance level reached by the term high vegetation indicates that this factor strongly affects temperature variation, proving that the correlation is not random.

Relief correlated moderately and positively with air temperature. In this regard, the temperature tends to be higher at higher, rather than lower, altitudes of the urban terrain. This relationship is expressive because the relief reached the adopted confidence interval, demonstrated by the *p*-value of 0.00.

In the joint analysis of the model with the adopted independent variables, the spatial model came closer to reality in the episode of 10 May 2020. This can be seen from the results obtained by the significance test that gave reliability to the spatialization of the UHI_{ucl}, both in air temperature recording sites and in discontinuous data areas. These results are supported by the correspondence between the features of land use and altimetry in distant areas of climate monitoring.

In the relationship between the recorded air temperature and the pixel-calculated radiative surface temperature, both extracted by the measured points (Table 3), the correlation is highly positive (0.93). This indicates that air temperature tends to be higher on the most heated surfaces, while in undergrowth vegetation sites the differences between air and surface temperatures are smaller, being practically null in areas with arboreal vegetation. In this relationship, the coefficient of determination was 0.88 and the confidence interval was fully reached.

Table 3. Results of the simple regression and ANOVA *p*-value ($\alpha \leq 0.05$) considering measured air temperature and surface temperature in Presidente Prudente on 10 May 2020.

Air Temperature X Surface Temperature	r	*p*-Value	Significant F Value	Adjusted R^2
Surface temperature	0.93	0.00	0.00	0.88

Data source: USGS (2021); Data recording on 10 May 2020. Organized by the authors, December 2021.

4. Discussion

The comparison between measured air temperature and the air temperature estimated by the multicriteria model showed slight differences (residues) in points 2 and 4, characterized by densely built-up areas. Thus, the model approached the reality of data recording. Furthermore, this variation in densely constructed points (2 and 4) suggests that unknown or unmonitored influences controlled the result in these places.

In the comparison between measured air temperature and surface temperature, greater thermal deviations occurred at 11 p.m. (local time) in the air and surface temperature extracted from urban fixed points (Figure 5). These points may undergo greater variations due to urban heterogeneities, as demonstrated by Xiong et al. [44]. These results reflect the differences between urban surfaces and surfaces with undergrowth and arboreal vegetation.

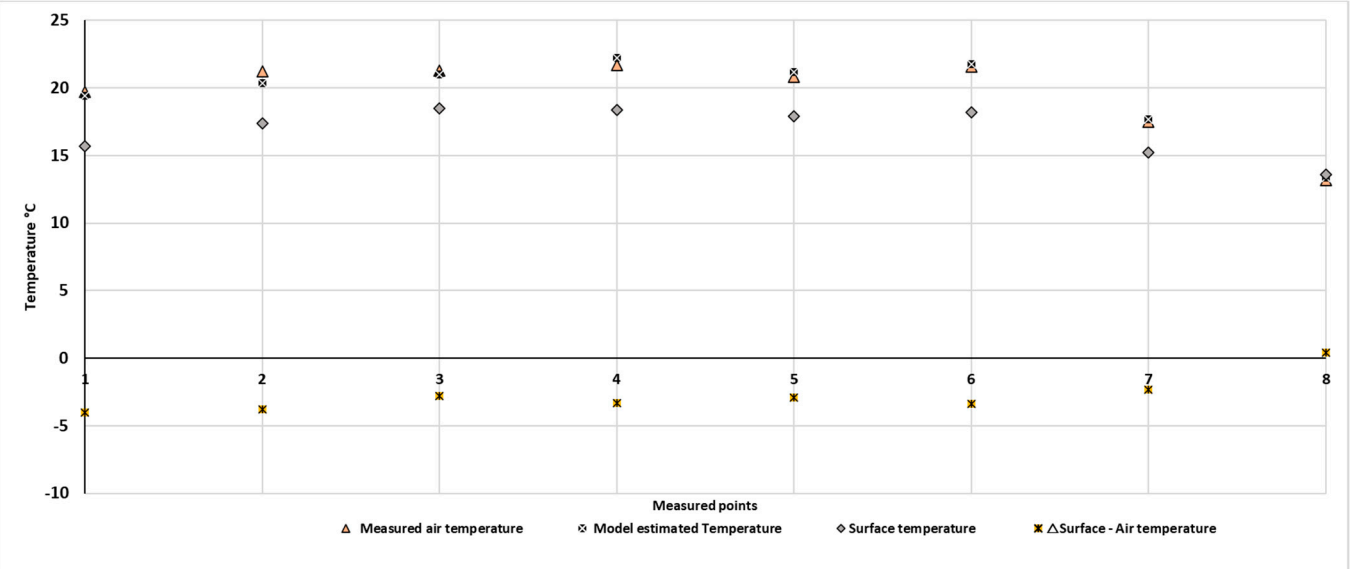

Figure 5. Measured air temperature (MAT), model-estimated temperature (MET), and surface temperature (ST) extracted from the measurement point, as well as the difference between measured and surface temperature (△ST–MAT). Data source: USGS (2021); data recording on 10 May 2020. Organized by the authors, December 2021.

The thermal response of urban materials present on the surface (urban targets captured by remote sensing, mostly characterized by watertight and little evaporative materials) shows lower thermal capacity for these components, which require less energy to heat up in the presence of radiation. However, urban surface components do not conserve energy

after sunset, providing heat to the adjacent atmosphere that becomes warmer than the surfaces [22,45].

Differently, vegetated areas showed little or no variation between air and surface temperature. Due both to the interception of radiation and to having greater thermal capacity, vegetation takes longer to heat up and slows down its cooling, keeping air–surface temperatures more constant. Point 8, characterized by dense vegetation cover, presented atmospheric heating content very close to the surface temperature pattern, assuming a difference of 0.4 °C in favor of the temperature of the target. This is because surfaces provided with undergrowth or arboreal vegetation transfer energy by the latent heat flow generated from evapotranspiration. Through this process, plants convert sensible heat into latent heat without adding heat to the atmosphere [42].

Less variation between measured air temperature and surface temperature also occurred in open areas, devoid of buildings, whose surfaces are characterized by undergrowth vegetation. This was the case for stations 1 and 3 and point 7. Meteorological stations at points 1 and 3 kept the ideal characteristics for the installation of equipment, but in recent years they have been incorporated into the urban fabric due to the territorial expansion of Presidente Prudente, as has happened to several cities in São Paulo State [46].

Given its location in the west of the urban grid, point 1 received the greatest influence from the sunset. This became evident at 5:50 p.m. (local time) on May 10, on the west–northwest horizon (https://www.vercalendario.info/pt/sol/brasil-mes-maio-2020.html, accessed on 12 January 2022). In association with the southwesterly wind direction, heating at this site was equivalent to that of built-up areas.

Unlike vegetated areas, built-up areas have a lower thermal capacity, assuming greater deviations between air and surface temperature. The literature explains this fact from the transport of surface heat towards the atmosphere after sunset [13]. Urban materials are thus the main heating sources modulating heat transfer to the atmosphere.

These results corroborate the classic profile of nocturnal UHI_{ucl} presented by Amorim (2020) [17] for Presidente Prudente city. In that study, the author used 26 fixed monitoring stations and daytime satellite images crossed with the temperature recorded at synoptic times (0 h, 3 h, 6 h, 9 h, 12 h, 15 h, 18 h, and 21 h) in 2 days of observation. Of this total of fixed points, eight composed the observation points of this article. The models generated by Amorim (2020), which used construction, high vegetation, and altitude variables, showed evidently higher overall correlations at night-time, especially at 9 p.m. (local time).

Presenting an advance in the procedure, in the present article we used satellite image, simultaneous in situ data recording, correlation analysis, and the significance test. Overall correlation indices showed correspondence in both studies, and the average of the overall coefficient obtained from the two episodes of the previous study was 0.91 at 9 p.m.

At 11 p.m., as shown in this article, the overall coefficient of the generated equation was 0.8. In addition, the significance test, which considered the *p*-value ($\alpha \leq 0.05$), proved that the relationship between the variables was not random or capricious.

5. Conclusions

Data recorded at the atmospheric level by the UHI_{ucl} study were crossed by a multicriteria linear regression model. This model estimated air temperature with proximity measures and mathematical reliability considering the different classes of land use and relief, assuming that these are important controls for the variation of air temperature on the local scale. In addition to the lower atmospheric level, the present study also included the analysis of UHI_{surf} through the application of remote sensing.

The combination of data involving reliable spatialization of UHI_{ucl} and UHI_{surf} enabled a comparative analysis between air temperature and the temperature of the targets as extracted by points of interest in the nocturnal episode of 10 May 2020.

The model efficiently estimated air temperature, as the temperatures in the eight points of interest enabled extrapolation of the information to discontinuous data areas with

similar surface characteristics, with mathematical confidence. The validation tests and the adopted *p*-value supported this result.

The model proves to be more advantageous than the general treatments performed by ordinary kriging that ignore the spatial variation of surface features. This is important for regions lacking broad and qualitative data coverage and which hinder the development of climate studies, especially fine-scale studies. The products generated and the validation of the results clearly demonstrated the configuration of UHI_{ucl} and UHI_{surf} in Presidente Prudente city, meeting the results of Amorim [17]. This author states that the greatest magnitude of the atmospheric heat island occurs at night, proving this through correlation coefficients that ranged from moderately to highly positive in the construction class and from moderately to highly negative for the high and low vegetation classes. The spatial variation of UHI_{ucl} and UHI_{surf} shows particularities that depend on the differentiated heating of surface features (vegetation, water, soils, buildings), on the diurnal variation in temperature, on prevailing meteorological conditions, and on other climate controls at a local scale (even on unknown or unsupervised influences).

In the simultaneous nocturnal analysis between air and surface temperature, UHI_{ucl} stood out in relation to UHI_{surf} due to the cooling of surfaces in the hours following sunset. This relationship is well defined in built-up areas, which transfer heat to the atmosphere close to the surface at night. Differently, vegetated surfaces are preserved warmer than the surfaces of built-up areas, with vegetation delaying surface cooling due to its capacity of converting sensible heat into latent heat from evapotranspiration, a process that does not add heat to the atmosphere. Depending on vegetation size, these areas will delineate minor or zero differences between air–surface temperatures.

The modulation of air temperature, as a function of surface temperature, reaching a coefficient of determination of 88%, allows us to infer that this relationship leaves 12% of doubt. This can be attributed to unmonitored influences at the atmosphere interface (wind speed and direction) or even to the generalization common to studies using remote sensing data. However, further studies may respond, either by adopting a larger number of observational fixed points or by incorporating local circulation schemes that can overcome the limitation of the air–target relationship.

Finally, we affirm that the model is applicable to other climate realities and we reiterate the importance of vegetation in the organization of urban spaces, mitigating the harmful effects of excess heat in urban areas, especially in the tropical continental environment.

Thus, planning urban surfaces becomes effective in mitigating the harmful effects of UHI. Reliable mappings can reflect positively on the composition of strategies and support governmental decision-making for urban planning to be resilient to the effects of urban climate.

Author Contributions: The authors conceived the experiments and designed the methodology. D.C.F.T. implemented the methodology, analyzed the results, and performed the statistical analysis and the final editing of images. M.C.d.C.T.A. provided the data from fixed data recording points, performed the geoprocessing, and supervised the project. All authors contributed to the interpretation of results and to the writing of the manuscript. All authors have read and agreed to the published version of the manuscript.

Funding: This research was funded by Brazilian National Council for Scientific and Technological Development (CNPq) for granting the Junior Postdoctoral scholarship (Process No. 151597/2020-0) and for the Productivity Research Grant (Process No. 307191/2018-4); to the CAPES/COFECUB Program (Process No. 88881.191765/2018-01) for financing the project titled Ciclamen: Cities, Climate, and Vegetation: Modeling and Environmental public policies; to the São Paulo Research Foundation—FAPESP (Processes: 2014/16350-3; 2015/50439-4. And the APC was funded through the authors' review vouchers.

Institutional Review Board Statement: Not applicable.

Informed Consent Statement: Not applicable.

Data Availability Statement: Not applicable.

Acknowledgments: The authors are grateful to São Paulo State University (UNESP), School of Technology and Sciences, Presidente Prudente Campus, for the institutional support; and to Universidade do Oeste Paulista (UNOESTE) for providing data from the Meteorological Station located at Universidade do Oeste Paulista, Campus 2, Presidente Prudente.

Conflicts of Interest: The authors declare that there is no conflict of interest.

References

1. Teixeira, D.C.F.; Amorim, M.C.C.T. Ilhas de calor: Representações espaciais de cidades de pequeno porte por meio de modelagem. *GEOUSP Espaço Tempo* **2017**, *21*, 239–256. [CrossRef]
2. Lang, S.; Blaschke, T. *Análise da Paisagem com SIG*; Kux, H., Translator; Oficina de Textos: São Paulo, Brazil, 2009.
3. Foissard, X. L'ilot de Chaleur Urbain et le Changement Climatique: Application a L'agglomeration Rennaise. Ph.D. Thesis, Universite de Rennes II, Rennes, France, 2015.
4. Foissard, X.; Dubreuil, V.; Quenol, H. Defining scales of the land use effect to map the urban heat island in a mid-size European city: Rennes (France). *Urban Clim.* **2019**, *29*, 100490. [CrossRef]
5. Amorim, M.C.C.T.; Dubreuil, V.; Cardoso, R.S. Modelagem espacial da ilha de calor urbana em Presidente Prudente (SP) Brasil. *Rev. Bras. Climatol.* **2015**, *16*, 29–45. [CrossRef]
6. Ortiz-Porangaba, G.F.; Teixeira, D.C.F.; Amorim, M.C.C.T.; Silva, M.H.S.; Dubreuil, V. Modeling the urban heat island at a winter event in Três Lagoas, Brazil. *Urban Clim.* **2021**, *37*, 100853. [CrossRef]
7. Oke, T.R.; Mills, G.; Christen, A.; Voogt, J.A. *Urban Climates*; Cambridge University Press: Cambridge, UK, 2017; pp. 14–43.
8. Amorim, M.C.C.T.; Dubreuil, V.; Amorim, A.T. Day and night surface and atmospheric heat islands in a continental and temperate tropical environment. *Urban Clim.* **2021**, *38*, 100918. [CrossRef]
9. Agathangelidis, I.; Cartalis, C.; Santamouris, M. Urban Morphological Controls on Surface Thermal Dynamics: A Comparative Assessment of Major European Cities with a Focus on Athens, Greece. *Climate* **2020**, *8*, 131. [CrossRef]
10. Gatto, E.; Ippolito, F.; Rispoli, G.; Oliver, S.C.; Santiago, J.L.; Aarrevaara, E.; Rohinton, E.; Buccolieri, R. Analysis of Urban Greening Scenarios for Improving Outdoor Thermal Comfort in Neighbourhoods of Lecce (Southern Italy). *Climate* **2021**, *9*, 116. [CrossRef]
11. Monteiro, C.A.F. Geographic climatology in Brazil and the proposal of a new paradigm. In *The Construction of Geographical Climatology in Brazil*; Alínea: Campinas, Brazil, 2015; pp. 61–153.
12. Lauwaet, D.; Maiheu, B.; De Ridder, K.; Boënne, W.; Hooyberghs, H.; Demuzere, M.; Verdonck, M.L. A New Method to Assess Fine-Scale Outdoor Thermal Comfort for Urban Agglomerations. *Climate* **2020**, *8*, 6. [CrossRef]
13. Oke, T.R. *Boundary Layer Climates*, 2nd ed.; Routledge: London, UK, 1987.
14. Garcia, F.F. *Manual de Climatologia Aplicada: Clima, Medio Ambiente y Planificacion*; Editorial Sintesis: Madrid, Spain, 1996.
15. Huang, F.; Zhan, W.; Voogt, J.; Hu, L.; Wang, Z.; Quan, J.; Ju, W.; Guo, Z. Temporal upscaling of surface urban heat island by incorporating an annual temperature cycle model: A tale of two cities. *Remote Sens. Environ.* **2016**, *186*, 1–12. [CrossRef]
16. Walker, J.J.; Beurs, K.M.; Henebry, G.M. Land surface phenology along urban to rural gradients in the U.S. Great Plains. *Remote Sens. Environ.* **2015**, *165*, 42–52. [CrossRef]
17. Amorim, M.C.C.T. Daily evolution of urban heat islands in a Brazilian tropical continental climate during dry and rainy periods. *Urban Clim.* **2020**, *34*, 100715. [CrossRef]
18. Cardoso, R.S.; Amorim, M.C.C.T. Variações espaciais das temperaturas noturnas em Presidente Prudente-SP em episódios de verão. *RA'E GA-Espaco Geogr. Anal.* **2017**, *42*, 257–268. [CrossRef]
19. Dorigon, L.P.; Amorim, M.C.C.T. Spatial modeling of an urban Brazilian heat island in a tropical continental climate. *Urban Clim.* **2019**, *28*, 100461. [CrossRef]
20. Pimentel, F.O.; Ferreira, C.C.M. Clima urbano: O uso de modelos geoespaciais na investigação do comportamento térmico em Juiz de Fora-MG. *Rev. Bras. Climatol.* **2019**, *24*, 49–66. [CrossRef]
21. Ferreira, C.C.M.; Pimentel, F.O.; Vianna, Y.C.G. Proposta Metodológica Aplicada ao Estudo de Clima Urbano. *Rev. Bras. Geogr. Física* **2019**, *12*, 2023–2040. [CrossRef]
22. Oke, T.R. The energetic basis of the urban heat island. *Q. J. R. Meteorol. Soc.* **1982**, *108*, 1–24. [CrossRef]
23. von Bertalanffy, L. *General System Theory: Foundations, Development, Applications, Ed. Reviewed*; George Braziller: New York, NY, USA, 1968; p. 289.
24. Porangaba, G.F.O.; Amorim, M.C.C.T. Analysis of diagnosed heat islands by means of mobile transects in Assis, Cândido Mota, Maracaí and Tarumã (SP). *Confins* **2017**, *33*. [CrossRef]
25. Giridharan, R.; Emmanuel, R. The impact of urban compactness, comfort strategies and energy consumption on tropical urban heat island intensity: A review. *Sustain. Cities Soc.* **2018**, *40*, 677–687. [CrossRef]
26. Jin, L.; Schubert, S.; Salim, M.H.; Schneider, C. Impact of air conditioning systems on the outdoor thermal environment during summer in Berlin, Germany. *Int. J. Environ. Res. Public Health* **2020**, *17*, 4645. [CrossRef]
27. Romano, P.; Prataviera, E.; Carnieletto, L.; Vivian, J.; Zinzi, M.; Zarrella, A. Assessment of the Urban Heat Island Impact on Building Energy Performance at District Level with the EUReCA Platform. *Climate* **2021**, *9*, 48. [CrossRef]
28. Short, J.R.; Farmer, A. Cities and Climate Change. *Earth* **2021**, *2*, 1038–1045. [CrossRef]

29. Dubreuil, V.; Fante, K.P.; Planchon, O.; Sant'Anna Neto, J.L. Climate change evidence in Brazil from Koppen's climate annual types frequency. *Int. J. Climatol.* **2018**, *1*, 1–14. [CrossRef]
30. Instituto Brasileiro de Geografia e Estatística (IBGE). Populacao Estimada. 2021. Available online: https://ibge.gov.br/cidades-e-estados/sp/presidente-prudente.html (accessed on 12 January 2022).
31. Environmental Systems Research Institute (ESRI). *ArcGis: World Imagery*; Environmental Systems Research Institute: Redlands, CA, USA, 2022.
32. Instituto Brasileiro de Geografia e Estatística (IBGE). Malha de Setor Censitário. 2010. Available online: https://ibge.gov.br/geociencias/organizacao-do-territorio/malhas-territoriais/26565-malhas-de-setores-censitarios-divisoes-intramunicipais.html?=&t=downloadshttps://cidades.ibge.gov.br/brasil/sp/presidenteprudente/panorama (accessed on 12 January 2022).
33. Voogt, J.A.; Oke, T.R. Thermal Remote Sensing of Urban Climates. *Remote Sens. Environ.* **2003**, *86*, 370–384. [CrossRef]
34. Weng, Q. Fractal Analysis of Satellite-Detected Urban Heat Island Effect. *Photogramm. Eng. Remote Sens.* **2003**, *69*, 555–566. [CrossRef]
35. Amorim, M.C.C.T. Spatial variability and intensity frequency of surface heat island in a Brazilian city with continental tropical climate through remote sensing. *Remote Sens. Appl. Soc. Environ.* **2018**, *9*, 10–16. [CrossRef]
36. United States Geological Survey (USGS). 2021. Available online: https://earthexplorer.usgs.gov/ (accessed on 25 August 2021).
37. Hobo Data Loggers. HOBO®Pro v2 (U23-00x) Manual. 2017. Available online: https://www.hobodataloggers.com.au/hobo-pro-v2-u23-002-external-temperaturerh-datalogger (accessed on 17 January 2022).
38. Instituto Nacional de Meteorologia (INMET). Estações Automáticas. 2020. Available online: https://mapas.inmet.gov.br/ (accessed on 17 January 2022).
39. Amorim, M.C.C.T. *Ilhas de Calor em Cidades Tropicais de Médio e Pequeno Porte: Teoria e Prática*, 1st ed.; Appris: Curitiba, Brazil, 2020; pp. 75–76.
40. Google Earth Pro. Available online: https://earth.google.com/web/ (accessed on 11 December 2021).
41. Jensen, J.R. *Introductory Digital Image Processing: A Remote Sensing Perspective*, 2nd ed.; Prentice Hall: Hoboken, NJ, USA, 1996.
42. Ferreira, M.C. *Iniciação a Analise Geoespacial: Teoria, Técnicas e Exemplos para Geoprocessamento*, 1st ed.; UNESP: São Paulo, Brazil, 2014; pp. 96–104.
43. Long, N.; Gardes, T.; Hidalgo, J.; Masson, V.; Schoetter, R. Influence of the urban morphology on the urban heat island intensity: An approach based on the Local Climate Zone classification. *PeerJ* **2018**, *6*, e27208v1. [CrossRef]
44. Xiong, K.; Yang, Z.; He, B.J. Spatiotemporal heterogeneity of street thermal environments and development of an optimised method to improve field measurement accuracy. *Urban Clim.* **2022**, *42*, 101121, preprints. [CrossRef]
45. Leeper, R.D.; Kochendorfer, J.; Henderson, T.A.; Palecki, M. Impacts of Small-Scale Urban Encroachment on Air Temperature Observations. *Am. Meteorol. Soc.* **2019**, *58*, 1369–1380. [CrossRef]
46. Fante, K.P. Variabilidade da Temperatura em Áreas Urbanas Não Metropolitanas do Estado de São Paulo-Brasil no Período de 1961 a 2011. Master's Thesis, Universidade Estadual Paulista, Presidente Prudente, São Paulo, Brazil, 2014.